Cellular and Molecular Biology
E-ISSN : 1165-158X / P-ISSN : 0145-5680
www.cellmolbiol.org

Original Research

Impact of citrate- and chitosan-capped gold nanoparticles on the liver of Swiss albino mice: Histological and cyto-genotoxic study

Eiman I. Zaki[1], Ayman S. El-Seedy[2*], Inaam P. Kelada[1], Nadia A. Sharafeldin[1], Hala M. Abdel Mouaty[1], Heba S. Ramadan[3]

[1] Histology and Cell Biology Department, Faculty of Medicine, Alexandria University, Alexandria, Egypt
[2] Laboratory of Cellular and Molecular Genetics, Genetics Department, Faculty of Agriculture, Alexandria University, Alexandria, Egypt
[3] Medical Biophysics Department, Medical Research Institute, Alexandria University, Alexandria, Egypt

[*]**Correspondence to:** ayman.el-seedy@alexu.edu.eg

Received October 22, 2018; **Accepted** May 15, 2019; **Published** June 30, 2019

Doi: http://dx.doi.org/10.14715/cmb/2019.65.5.3

Abstract: The present study aimed to disclose the histological alterations and cyto-genotoxic potential induced by citrate- and chitosan-capped AuNPs on liver of adult Swiss albino mice. Animals were randomly divided into 8 groups. The first two groups were intraperitoneally (i.p) injected with physiological saline once and left for 10 days and every other day for 21 days, respectively, and kept as negative control groups. While the third and fourth groups were injected i.p with a single dose of 2 mg/kg of citrate- and chitosan-capped AuNPs, respectively, and left for 10 days. The fifth and sixth groups were injected i.p every other day for 21 days with 200 µg/kg of citrate- and chitosan-capped AuNPs, respectively. Animals of the seventh and eighth groups were injected i.p with 50 mg/kg cyclophosphamide once and left for 10 days and with 20 mg/kg cyclophosphamide every other day for 21 days, respectively. The livers of mice were dissected and processed for microscopic examination and for analyzing the expression of inflammation-related genes using RT-PCR. In addition, bone marrow samples were taken to investigate the mitotic index and the chromosomal aberrations. The present study showed various degrees of structural changes in the liver of animals received AuNPs. Such changes were more prominent in animals treated with a single dose of AuNPs, particularly with citrate-capped AuNPs as compared to chitosan-capped AuNPs. Furthermore, genotoxic analysis did not reveal any genotoxicity for AuNPs with both coats. Therefore, chitosan-capped AuNPs were less hepatotoxic than citrate-capped ones. However, it has not been proven that AuNPs are genotoxic by both coats.

Key words: Gold nanoparticles; Chitosan; Citrate; Histology; Genotoxicity; Liver; Mice.

Introduction

Nanotechnology is the technology dealing with the matter at a small scale with a diameter smaller than 100 nm (1). It is applied on different levels starting from materials passing by devices reaching to systems. The nanomaterials level is the most advanced at present, both in scientific and in commercial applications (2). Nanoparticles are defined as being smaller than 100 nm in at least one dimension (3). They are used in different medical applications, including drug carrier systems, (4) and tissue engineering (5).

In general, the nanosize of nanoparticles permits them to enter to different cells and cellular components, which may lead to some hazardous and toxic effects depending on various factors such as size, shape, composition and surface functionalization (6). There has been an increasing interest in the use of gold nanoparticles (AuNPs) in the field of medicine. AuNPs are one of the promising nanoparticles (NPs) in diagnostic and therapeutic purposes (2). They have special optical properties as they have unique interaction with light. Although gold is considered to be inert, AuNPs exhibit higher reactivity as a result of the high surface area to volume ratio at a nanoscale, which may accordingly increase their toxicological outline (7).

Functionalization (coating or capping) of nanomaterials with different molecules is a useful trend to prepare new materials with more beneficial properties. Functional groups on NPs surfaces are main director of many important properties, such as solubility and interactions with cell surface (8). Similarly, AuNPs with different capping may behave in different ways at cellular level by interacting with cell membrane, mitochondria or nucleus and can impart adverse effects like organelle or DNA damage (9). Capping of the AuNPs could help making the particles more biocompatible (10). Thus, synthesizing AuNPs with lesser toxicity is now one of the primary interests in the field of nanotechnology (11). Citrate is used as the classical chemical for preparing AuNPs, giving them an anionic coat (12). Chitosan is a polysaccharide derivative of chitin. It has been included into medical research and applications due to its low toxicity, high biocompatibility and its ability to interact and permeate cellular membranes (13). Chitosan conjugated to AuNPs has been presented as a suitable tool for biosensing (14) in drug delivery (10), as antibacterial (15) and antifungal agents (16), and for tumor targeting (17). According to biodistribution studies, liver was reported as one of the organs that AuNPs accumulate

mostly in after systemic administration, showing the importance to evaluate AuNPs toxicity on such tissue (18).

Great deal of attention has been paid to evaluate the impact of both natural and unnatural nanomaterials used in medical applications. For AuNPs there are few studies about their genotoxicity, in addition that the existing reports are still questionable. Some have reported that AuNPs could cause DNA damage *in vitro* and *in vivo* (19, 20). While others, did not record any obvious genotoxic damage from AuNPs *in vitro* and *in vivo* experiments (21-23). The present study therefore aimed at disclosing the potential histological changes in the liver of adult Swiss albino mice as well as cyto-genotoxicity induced by AuNPs coated by two different coats; citrate as a chemical anionic coat, and chitosan as a natural cationic one.

Materials and Methods

Synthesis of AuNPs

AuNPs of 80 to less than 100 nm in size were used in this work. Citrate capped AuNPs were synthesized as described by McFarland et al. (24), 20 ml of 1.0 mM chloroauric acid ($HAuCl_4$) were prepared and the solution was heated till boiling. Then, 2 ml of a 0.4% solution of trisodium citrate dihydrate ($Na_3C_6H_5O_7.2H_2O$) were added as a reducing agent. It was removed from heat when it turned deep red. While chitosan- capped AuNPs were synthesized by preparing a solution of 100 ml of $1.25x10^{-1}$ M of $HAuCl_4$ (25). The solution was boiled and 100 ml of a 0.2% solution of chitosan prepared in 1% acetic acid were added as reducing agent. When the solution has turned deep red, it was removed from heat.

All chemicals were purchased from Sigma-Aldrich (St. Louis, MO, USA). The mean particle size and surface charge (zeta potential) of AuNPs were determined using Nano-Zeta sizer particle analyzer (Malvern, UK). The wavelength of highest absorption was determined using ultraviolet UV-6800UV\VIS Spectrophotometer (Jenway–Germany). The shape and size of the prepared nanoparticles were determined by transmission electron microscope (TEM) (Jeol 100 CX, Tokyo, Japan).

Ethics statement

Maintenance of animals, experimental design and investigation protocols were approved by Ethics Committee, Faculty of Medicine, Alexandria University (ECFM-AU/SN-020513), in accordance with the guide for care and use of laboratory animals in research. Mice used in this study were acclimatized for two week before the beginning of the experiment and all efforts were made to minimize animal suffering during the investigation procedures.

Animals and treatment protocols

The study was conducted on 140 Swiss albino adult male mice, aged 2-3 months and weighing 30-40 grams. The animals were maintained under standard laboratory conditions of temperature and humidity and 12 hours light/dark cycle. Water and feed were provided ad libitum. The mice were fed with standard mouse pellets.

Animals were randomly divided into 8 groups. The first two groups were intraperitoneally (i.p) injected with physiological saline once and left for 10 days and every other day for 21 days, respectively, and kept as negative control groups. While the third and fourth groups were injected i.p with a single dose of 2 mg/kg of citrate- and chitosan-capped AuNPs, respectively, and left for 10 days (26). The fifth and sixth groups were injected i.p every other day for 21 days with 200 µg/kg of citrate- and chitosan-capped AuNPs, respectively (27). Animals of the seventh and eighth groups were injected i.p with 50 mg/kg cyclophosphamide once (28) and left for 10 days and with 20 mg/kg cyclophosphamide every other day for 21 days (29), respectively, and kept as positive control groups for genotoxic evaluation. At the end of the experiment, mice were sacrificed and livers were dissected and processed for microscopic examination and for analyzing the expression of inflammation-related genes, such as IL-1ß, IL-6, TNF-α, iNOS and COX-2 using RT-PCR. Also, bone-marrow samples were taken to analyze chromosomal aberrations and mitotic index whereas blood samples were obtained to assess the biomarker enzymes, such as aspartate aminotransferase (AST) and alanine aminotransferase (ALT).

Histological examination

Livers were excised and cut into 2 specimens, one was immediately cut into small pieces (1/2-1 mm^3), fixed in 3% gluteraldehyde solution and processed to get ultrathin sections for TEM examination (30). The other specimen was fixed in 10% formol saline, processed to get 6 µm thick paraffin sections and then stained with H&E stain for light microscopic examination (31, 32).

Activity of transaminases

Blood samples were collected from the retro-orbital venous plexus of animals early in the morning before feeding on the day of sacrifice, allowed to stand undisturbed for 2 hours and then centrifuged at 3000 r/min for 10 min. Serum was separated and stored at -80°C. The activity of aspartate aminotransferase (AST) and alanine aminotransferase (ALT) was measured spectrophotometrically in serum by the method of Chaisera et al. (33) using commercial kits (Diamand diagnostics, MDSS GmbH, Germany). Enzyme activity was checked for accuracy by concurrent analysis of control sera for ALT and AST and expressed as International Units per liter (IU/l).

Gene expression analysis

The biomarker expressions of mRNAs for the inflammation-related genes (pro-inflammatory genes) such as IL-1, IL-6, TNF-α, iNOS and COX-2 genes expression were carried out by using RT-PCR assay (34). Total RNA extraction was isolated from mouse liver tissues (approximately 30 mg) using EZ-10 Spin Column Total RNA Mini-Preps Kit (Bio Basic Inc., Markham, ON, Canada). The extracted RNA was dissolved in 30 µL nuclease-free distilled water and stored at -20°C. RT-PCR was performed in a single step reaction using Verso-1-Step–RT-PCR Hot Start kit (Thermo Scientific) on 30 ng of total RNA using the respective primers (Table 1). RT-PCR amplifications were performed using a Biometra thermal cycler (Biometra, Germany) under the following cycling conditions: 25-28 cycles of 94°C

Table 1. Primer sequences of inflammation-related genes employed for the genetic analysis of citrate- and chitosan-capped gold nanoparticles.

Primer name	Nucleotide sequence	
	Forward (5'-3')	Reverse (5'-3')
IL-1ß	CAGGATGAGGACATGACACC	CTCTGCAGACTCAAACTCCAC
iNOS	AGCTCCTCCCAGGACCACAC	ACGCTGAGTACCTCATTGGC
TNF-α	TTGACCTCAGCGCTGAGTTG	CCTGTAGCCCAGGTCGTAGC
COX-2	AAGAAGAAAGTTCATTCCTGATCCC	TGACTGTGGGAGGATACATCTCTC
IL-6	GTACTCCAGAAGACCAGAGG	TGCTGGTGACAACCACGGCC
Actin	GGCGGACTATGACTTAGTTG	AAACAACAAATGTGCAATCAA

for 1 min, 55°C for 1 min, and 72°C for 1 min. PCR products were loaded on a 2% agarose gel and band intensity was analyzed using Scion Image software (release Alpha 4.0.3.2, NIH). Actin mRNA was used as a housekeeping gene.

Analysis of chromosomal aberration in bone marrow cells and mitotic index (MI) assay

This assay characterizes any gross structural or numerical chromosomal alterations induced by AuNPs. On the day of scarification, animals were injected by colchicine in tail vein to arrest the cell cycle at metaphase. The bone marrow cells were collected from both tibiae according to Brusick (35), transferred to phosphate buffered saline, centrifuged and then slides were prepared and stained with Giemsa stain. Bone marrow samples were subsequently analyzed by the light microscope using oil emersion lens (1000X) to assess the mitotic index and chromosomal abnormalities based upon their individual structure and number. For each mouse, 1000 cells were counted and the mitotic index was computed as the ratio of the dividing cells to the total examined cells multiplied by 100.

Statistical analysis and scoring of data

Data are expressed as Mean ± SEM. Statistical analysis was performed using IBM SPSS software package version 20.0 (36). Analysis of variance (ANOVA) and Student's -test were used to assess the variability among treatment groups. The distributions of quantitative variables were tested for normality using Kolmogorov-Smirnov, Shapiro-Wilk and D'Agstino tests. Post Hoc test (LSD) and Tukey were used for comparison among different treatment groups. For abnormally distributed data, comparison were done using Mann Whitney test while Kruskal Wallis test was used to compare between different groups and pair wise comparison was assessed using Mann-Whitney. Significance of the obtained results was judged at *p<0.05, **p<0.01.

Results

Characterization of citrate-capped and chitosan-capped AuNPs

TEM imaging of AuNPs showed that they were spherical in shape with smooth surface, where the citrate-capped AuNPs were in the size range of 70.6-90.8 nm (Figure 1a) and the chitosan-capped AuNPs in the size range of 76.6-97.6 nm (Figure 1b). UV-visible spectrophotometer revealed that the plasmon absorption of the prepared AuNPs was clearly visible with maximum absorption peak at 550 nm (Figure 2a) and 548 nm (Figure 2b) for citrate- and chitosan-capped AuNPs, respectively. Nano Zeta sizer particle analyzer revealed

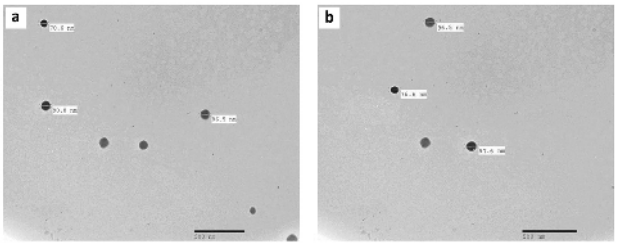

Figure 1. (a) Electron micrograph of citrate-capped AuNPs of size range 70.6-90.8 nm **(b)** Electron micrograph of chitosan-capped AuNPs of size range 76.6-97.6 nm.

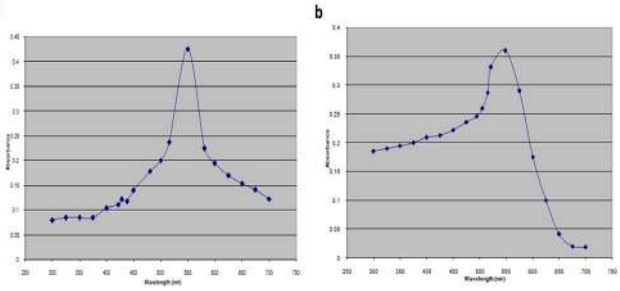

Figure 2. (a) Absorption spectrum of citrate-capped AuNPs (*λmax= 550 nm*) **(b)** Absorption spectrum of chitosan-capped AuNPs (*λmax= 548 nm*).

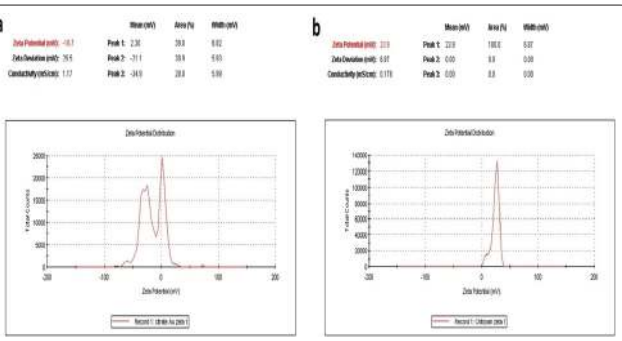

Figure 3. (a) Zeta Potential curve for citrate- capped AuNPs. **(b)** Zeta Potential curve for chitosan- capped AuNPs.

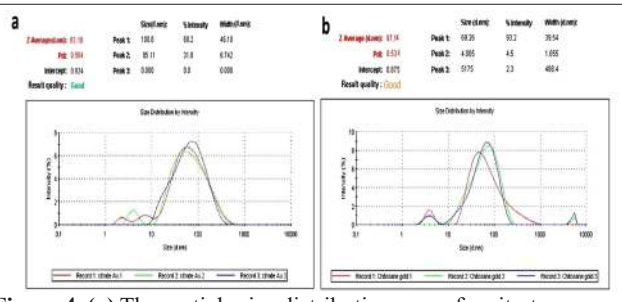

Figure 4. (a) The particle size distribution curve for citrate- capped AuNPs. **(b)** The particle size distribution curve for chitosan- capped AuNPs.

that the mean zeta potential of citrate- and chitosan-capped AuNPs was -16.7 and 23.9, respectively (Figure 3). While, the mean particle size was 93.18 nm for citrate-capped AuNP (Figure 4a) and 97.14 nm for chito-

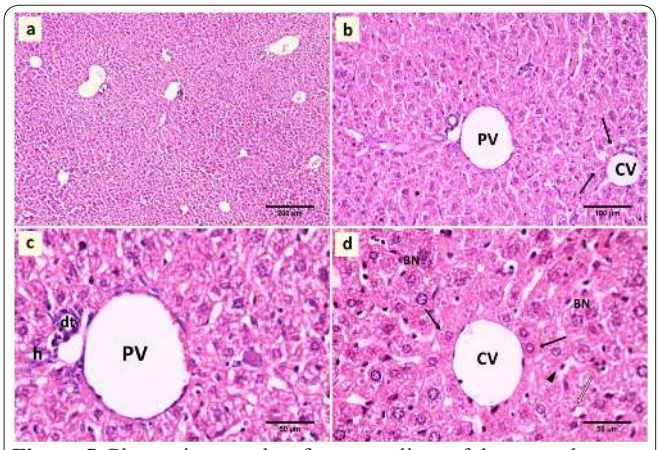

Figure 5. Photomicrographs of a mouse liver of the control groups (first and second groups), received physiological saline. **(a)** Photomicrograph of normal mouse liver architecture. **(b)** Photomicrograph shows cords of hepatocytes (black arrow) radiating from central vein (CV). PV; a branch of portal vein in portal tract. **(c)** A higher magnification of photomicrograph (b); showing components of portal tract; branch of the portal vein (PV), branch of the hepatic artery (h) and a bile duct (dt). **(d)** Photomicrograph shows hepatocytes (black arrow) arranged in cords radiating from central vein (CV) separated by blood sinusoids lined by endothelial cells (white arrow) and Von Kupffer cells (arrow head). They are polyhedral in shape with slightly vacuolated acidophilic granular cytoplasm and vesicular nuclei. Some binucleated hepatocytes are also seen (BN). (H&E stain).

san-capped AuNPs (Figure 4b).

Histological results

Light microscopic examination of the liver sections of control groups (first and second group) revealed almost the same normal hepatic architecture; the hepatic lobules appeared to be made up of hepatocytes arranged in cords radiating from the central veins. The hepatocytes are polyhedral in shape with granular acidophilic cytoplasm and rounded vesicular centrally located nuclei, some cells were binucleated. In between the hepatic cords, the hepatic sinusoids appeared as narrow spaces lined by flattened endothelial cells and Von Kupffer cells. The portal tracts were seen at the periphery of the hepatic lobules. They showed one bile duct radical, a branch of the hepatic artery and a branch of the portal vein, all are enclosed by scanty amount of connective tissue (Figure 5).

Animals injected with AuNPs showed various degrees of structural changes in the liver. The liver sections of animals injected with a single dose of 2 mg/kg citrate-capped AuNPs and left for 10 days showed many areas of disturbed hepatic architecture. Portal tracts showed dilated and congested branches of portal vein as well as dilatation and proliferation of bile ducts. Mononuclear cellular infiltration was seen around portal tracts and in between hepatocytes. Moreover, there was dilatation of blood sinusoids with numerous Von Kupffer cells. Hepatocytes showed either hypereosinophilic, vacuolated or dark homogenous cytoplasm. Some hepatocytes' nuclei were enlarged, others were karyolytic, few were pyknotic and some showed margination of chromatin. Many binucleated cells were noticed (Figure 6).

Liver sections of animals received 2 mg/kg of chito-

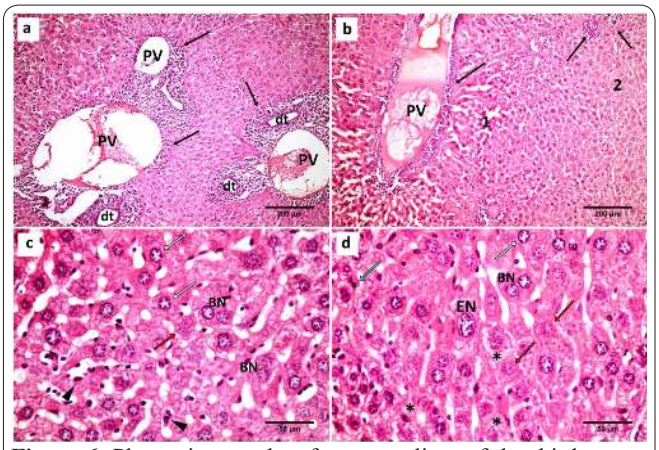

Figure 6. Photomicrographs of a mouse liver of the third group, received single dose (2 mg/kg) of citrate-capped AuNPs. **(a,b)** Photomicrographs show disturbed liver architecture. Portal tracts show dilated and congested branches of portal vein (PV) and dilatation and proliferation of bile ducts (dt). Intercellular and periportal mononuclear cellular infiltration are noticed (black arrow). Area (1) shows wide sinusoids while area (2) has narrower ones. **(c,d)** Photomicrographs show hypereosinophilic hepatocytes. Some hepatocytes are swollen with vacuolated cytoplasm (*) and few with dark homogenous cytoplasm and pyknotic nuclei (blue arrow). Nuclei with marginated chromatin giving it a ring shape appearance (white arrow), karyolitic (red arrow) and large nuclei (EN) are also noticed. Sinusoids are dilatated with numerous Von Kupffer cells (arrow head). Binucleated hepatocytes (BN) are noticed. (H&E stain).

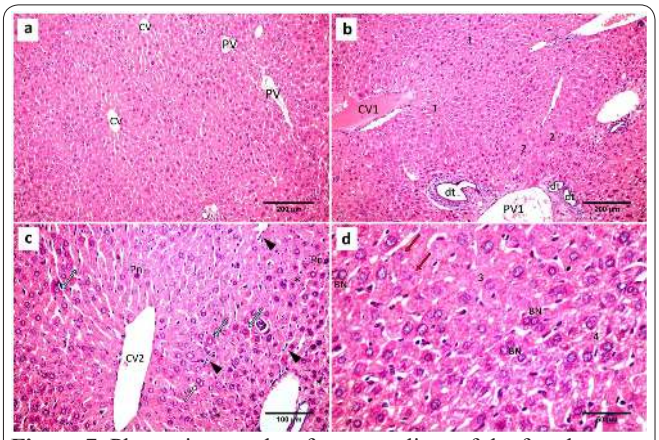

Figure 7. Photomicrographs of a mouse liver of the fourth group, received single dose (2 mg/kg) of chitosan-capped AuNPs. **(a)** Photomicrograph shows normal liver architecture. CV; central vein, PV; branch of portal vein. **(b)** Photomicrograph shows dilated congested central veins (CV1) surrounded by mononuclear cellular infiltration. Portal areas show dilatation of branches of portal vein (PV1) and proliferated dilated bile ducts (dt) surrounded by mononuclear cellular infiltration. Notice mild dilatation of blood sinusoids in areas (1) compared to narrower or even obliterated ones in areas (2). **(c)** Photomicrograph shows a dilated central vein (CV2). Blood sinusoids are dilated with many Von Kupffer cells (arrow head). Hepatocytes show hypereosinophilia with dark homogenous cytoplasm in some cells (blue arrow) and vacuolation in others (*). Hepatocytes with marginated heterochromatin (white arrow) and pyknotic nuclei (Pn) are noticed. **(d)** Photomicrograph shows many binucleated hepatocytes (BN). Hepatocytes in area (3) have hypereosinophilic granular cytoplasm while in area (4) have vacuolated cytoplasm. Notice hepatocytes with karyolytic nuclei (red arrow). (H&E stain).

san-capped AuNPs as a single dose and left for 10 days, showed nearly preserved liver architecture (Figure 7a)

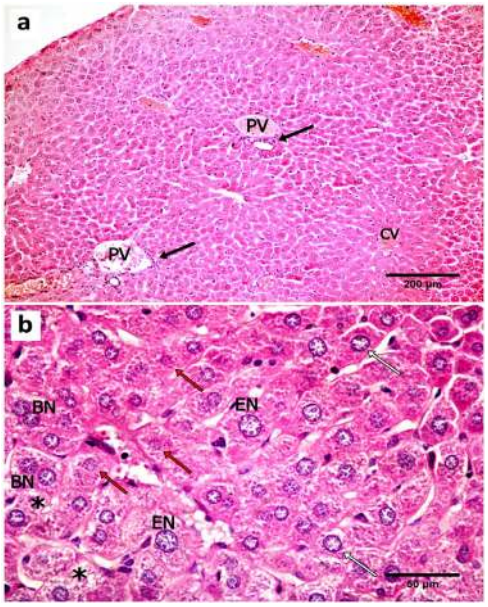

Figure 8. Photomicrographs of a mouse liver of the fifth group, received repeated doses of (200 µg/kg) citrate-capped AuNPs. **(a)** Photomicrograph shows normal liver architecture with minimal periportal mononuclear cellular infiltration (black arrow). The branches of portal veins (PV) and the central veins (CV) are mostly of normal caliber but show congestion. Hepatocytes show hypereosinophilia. **(b)** Photomicrograph shows hepatocytes with enlarged nucleus (EN), margination of nuclear chromatin (white arrow) and karyolytic nuclei (red arrow). Swollen hepatocytes with vacuolated cytoplasm (*) and binucleated cells (BN) are well noticed. (H&E stain).

except for few areas revealed findings similar to animals received 2 mg/kg of citrate-capped AuNPs (Figure 7b-d). Whereas, the liver sections of animals received every other day 200 µg/kg of citrate- and chitosan-capped AuNPs for 21 days revealed almost preserved liver architecture except for few focal areas showed changes similar to animals received 2 mg/kg of citrate-capped AuNP (Figures 8-9).

Electron microscopic examination of liver of control group showed normal hepatocytes with nuclei of regular smooth contour and prominent nucleoli. The cytoplasm showed intact organelles including numerous mitochondria and multiple arrays of rER (rough endoplasmic reticulum) in addition to glycogen particles appeared as electron dense aggregates. Few lipid droplets and few vacuoles were also noticed. Bile canaliculi were seen with microvilli protruding into the lumen enclosed between two adjacent hepatocytes and firmly bounded by desmosomes. Perisinusoidal space of Disse was observed with many microvilli of hepatocytes protruding into it. Von Kupffer cells with heterochromatic irregular nuclei, many lysosomes and vacuoles were seen lining the blood sinusoids (Figure 10). On the other hand, groups received AuNPs showed various degrees of changes in the hepatocytes. In animals injected with 2 mg/kg of citrate-capped AuNPs, hepatocytes showed different changes, where rarefaction of the cytoplasm and mitochondria with either bizarre shaped, swollen or dense with unapparent cristae were noticed. Also, endoplasmic reticulum was proliferated. Lysosomes containing electron dense materials most probably AuNPs were seen as well. Some hepatocytes' nuclei were shrunken showing condensed chromatin and irregular

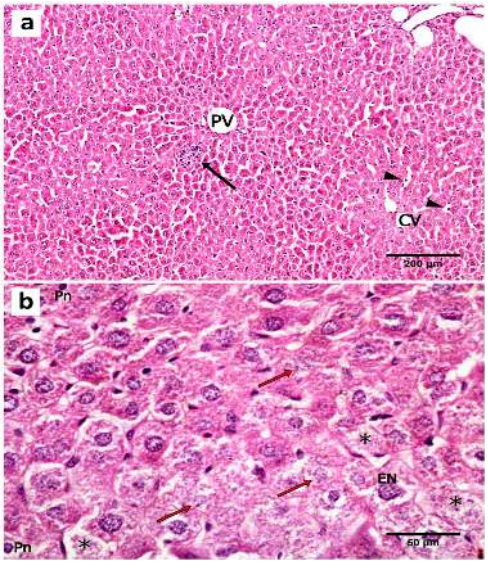

Figure 9. Photomicrographs of a mouse liver of the sixth group, received repeated doses of (200 µg/kg) chitosan-capped AuNPs. **(a)** Photomicrograph shows preserved liver architecture with minimal focal mononuclear cellular infiltration in between hepatocytes (black arrow). The branch of portal vein (PV) and the central vein (CV) appear normal while hepatocytes show hypereosinophilia. Notice areas showing sinusoidal dilatation with apparently increased number of Von Kupffer cells (arrow head). **(b)** Photomicrograph shows ballooned hepatocytes with cytoplasmic vacuolation (*) Notice hepatocytes with karyolytic nuclei (red arrow), enlarged nuclei (EN) and pyknotic nuclei (Pn). (H&E stain).

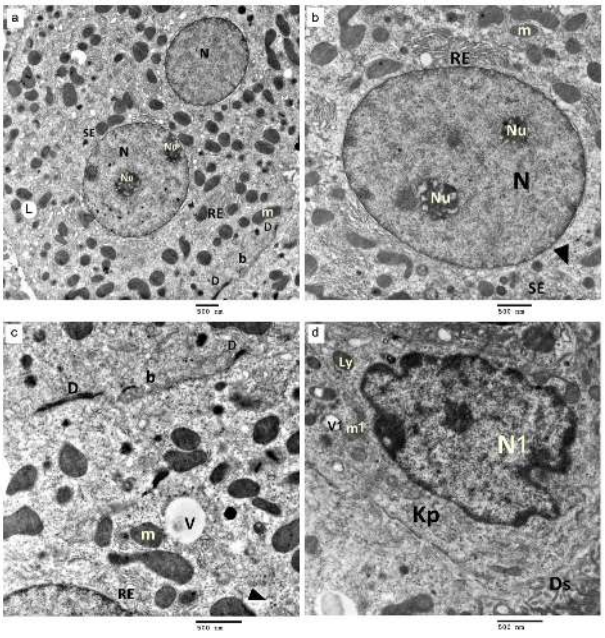

Figure 10. Electron micrographs of a mouse liver of the control groups (first and second groups), received physiological saline. **(a)** Electron micrograph shows a binucleated hepatocyte. **(a,b,c)** Electron micrographs show euchromatic nuclei (N) of regular outline and visible nucleoli (Nu). The cytoplasm shows parallel arrays of rER (RE), sER (SE), numerous mitochondria (m), glycogen granules (arrow head), lipid droplets (L) and vacuoles (V). Notice bile canaliculus (b) enclosed between two adjacent hepatocytes and bounded by desmosomes (D). **(d)** Electron micrograph shows a Von Kupffer cell (Kp) lining the blood sinusoid. It has heterochromatic irregular nucleus (N1) and its cytoplasm shows lysosomes (Ly), vacuoles (V1) and some mitochondria (m1). Part of a hepatocyte is seen with many microvilli protruding into the space of Disse (Ds). (Uranyl acetate/lead citrate stain).

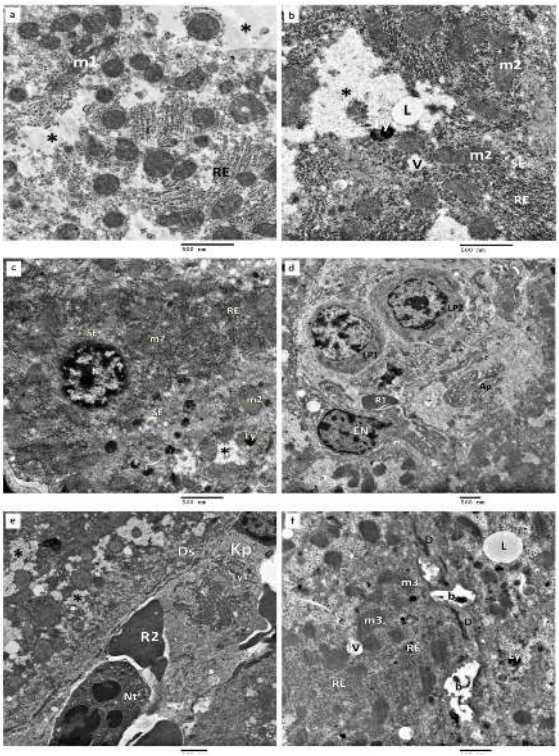

Figure 11. Electron micrographs of a mouse liver of the third group received single dose of (2mg/kg) citrate-capped AuNPs. **(a,b,c)** Electron micrographs show hepatocytes with rarified cytoplasm (*), lysosome (Ly) with electron dense material, bizarre-shaped (m1) and swollen mitochondria (m2). **(c)** Electron micrograph revealing a hepatocyte with a small nucleus (N) having a condensed chromatin and irregular outlines. **(d)** Electron micrograph shows endothelial cell (EN) lining the blood sinusoid. Notice apoptotic body (Ap), red blood cell (R1) and lymphocytes (LP1, LP2) in the blood sinusoid. **(e)** Electron micrograph shows a large Von Kupffer cell (Kp) lining the sinusoid with lysosomes inside it (Ly1). Notice rarified cytoplasm of an adjacent hepatocyte (*). **(f)** Electron micrograph shows dilated bile canaliculi (b) with short microvilli protruding into the lumen. The hepatocytes' cytoplasm revealing bizarre shaped dense mitochondria with unapparent cristae (m3) and lysosomes (Ly) with electron dense materials. RE; rER, SE; sER, R2; red blood cell**,** Nt; neutrophil, Ds; space of Disse, L; lipid droplets, V; vacuole, D; desmosome. (Uranyl acetate/lead citrate stain).

outline. Apoptotic bodies containing aggregated cytoplasmic organelles were seen inside blood sinusoids. Dilated bile canaliculi with few microvilli protruding into the lumen enclosed between two adjacent hepatocytes and bounded by desmosomes were seen. The Von Kupffer cells lining blood sinusoids were hypertrophied and revealed heterochromatic nuclei and multiple lysosomes (Figure 11).

In animals injected with 2 mg/kg of chitoson-capped AuNPs, the cytoplasm of some hepatocytes was denser when compared to adjacent hepatocytes revealing the dark-light cell phenomena. Many mitochondria were swollen and only some showed dense matrix with unapparent cristae. Endoplasmic reticulum was proliferated where rER (RE) was partially degranulated and sER (SE) was dilated. Lysosomes showed similar changes as animals injected with 2 mg/kg of citrate-capped AuNPs. Some of the hepatocytes' nuclei were shrunken with irregular outlines, some showed deep indentations while others showed margination of heterochromatin

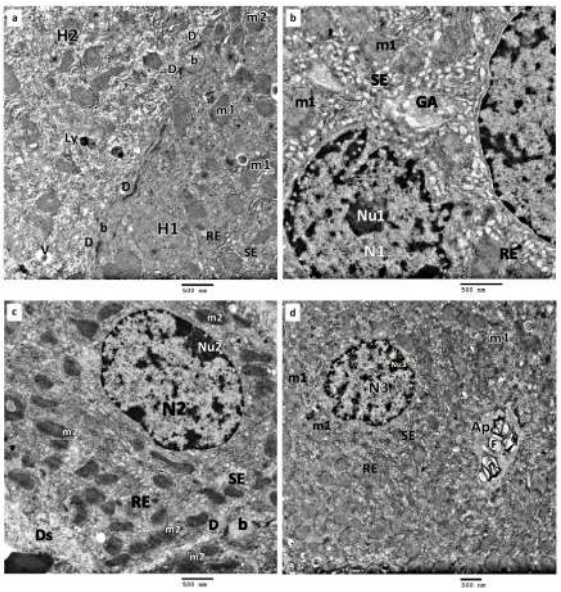

Figure 12. Electron micrographs of mouse liver of the fourth group, received single dose of (2 mg/kg) chitosan-capped AuNPs. **(a-d)** Electron micrographs show proliferated endoplasmic reticulum where rER (RE) is partially degranulated and sER (SE) is dilated. Swollen (m1), dense (m2) mitochondria and lysosomes (Ly) with electron dense materials are noticed. **(a)** Electron micrograph shows part of two adjacent hepatocytes enclosing dilated bile canaliculi (b) with microvilli protruding into the lumen and bounded by desmosomes (D). Notice denser cytoplasm in hepatocye (H1) when compared to hepatocyte (H2). V; vacuole**. (b)** Electron micrograph revealing binucleated hepatocyte, one of the nuclei (N1) shows deep indentations with margination of heterochromatin and apparent nucleolus (Nu1). Notice dilated stalks of Golgi apparatus (GA). **(c)** Electron micrograph revealing a hepatocyte with marginated nucleolus (Nu2). N2; a nucleus with marginated chromatin. Ds; space of Disse. **(d)** Electron micrograph shows a hepatocyte with shrunken irregular nucleus (N3) and marginated nucleolus (Nu3). Myelin figures (F) in an apoptotic body (Ap) are noticed. (Uranyl acetate/lead citrate stain).

and margination of nucleoli. In addition, dilated bile canaliculi and apoptotic bodies containing myelin figures were revealed (Figure 12).

Moderate changes in the cytoplasm and the nuclei were noticed in animals received 200 µg/kg of either citrate- or chitoson-capped AuNPs for 21 days. The cytoplasm of only few hepatocytes revealed the dark-light cell phenomena (Figures 13, 14). Animals received 200 µg/kg chitoson-capped AuNPs for 21 days showed multiple hepatocytes' nuclei with margination of nucleoli (Figure 14a).

AST and ALT levels

The mice injected by citrate- and chitosan-capped AuNPs at 2 mg/ kg once and left for 10 days showed, significantly increased mean serum levels of AST and ALT, while mice injected every other day with citrate- and chitosan-capped AuNPs at 200 µg/kg for 21 days showed no significant increase in the mean serum levels of AST and ALT when compared to control group (received physiological saline) (Table 2). However no significant differences were noticed in mean serum levels of AST and ALT when comparing the groups injected by citrate-capped to those injected by chitosan-capped AuNPs. Mean serum levels of AST and ALT in mice

Table 2. Biochemical parameters in mice exposed to citrate- and chitosan-capped AuNPs ; single and repeated doses.

Groups	Single dose		Repeated doses	
	AST	ALT	AST	ALT
Control group	12.51 ± 2.15*	4.59 ± 0.88*	10.50 ± 1.75	5.65 ± 1.52
Citrate- capped AuNPs	30.12 ± 5.02*	14.40 ± 2.88*	11.08 ± 2.02	5.60 ± 1.60
Chitosan- capped AuNPs	25.19 ± 2.51*	10.93 ± 0.92*	10.50 ± 4.63	5.33 ± 1.67

AST: Aspartate transaminase (unit/ml); ALT: Alanine transaminase (unit/ml). Data was represented as mean ± SD. Significance of difference where all treated groups were compared with control group (received physiological saline) at P<0.05*.

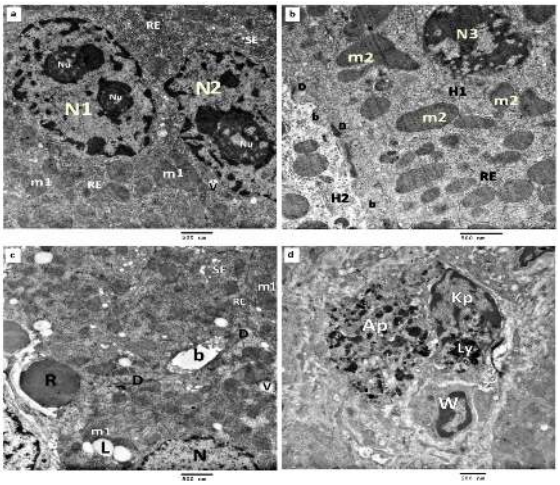

Figure 13. Electron micrographs of mouse liver of the fifth group, received repeated doses of (200 µg/kg) citrate-capped AuNPs. **(a-c)** Electron micrographs show hepatocyte with swollen (m1) and bizarre shaped enlarged mitochondria with unapparent cristae (m2). Dilated sER (SE) is also seen. **(a)** Electron micrograph shows a binucleated hepatocyte. The nuclei (N1), (N2) and (N) depict irregular outlines and margination of the chromatin. **(b)** Electron micrograph shows two adjacent hepatocytes, hepatocyte (H1) shows denser cytoplasm when compared to the cytoplasm of hepatocyte (H2). H1 exhibits shrunken nucleus (N3) with a condensed chromatin. **(b,c)** Dilated bile canaliculi (b) bounded by desmosomes (D) are seen. **(d)** Electron micrograph shows an apoptotic body (Ap) with electron dense substances inside it. A shrunken small cell (W) with heterochromatic nucleus is noticed inside a blood sinusoid. An active Von Kupffer cell (Kp) with irregular heterochromatic nucleus and lysosomes (Ly) with electron dense substance is seen. RE; rER, Nu; nucleolus, L; lipid droplet, V; vacuole, R; Red blood cell in blood sinusoid. (Uranyl acetate/ lead citrate stain).

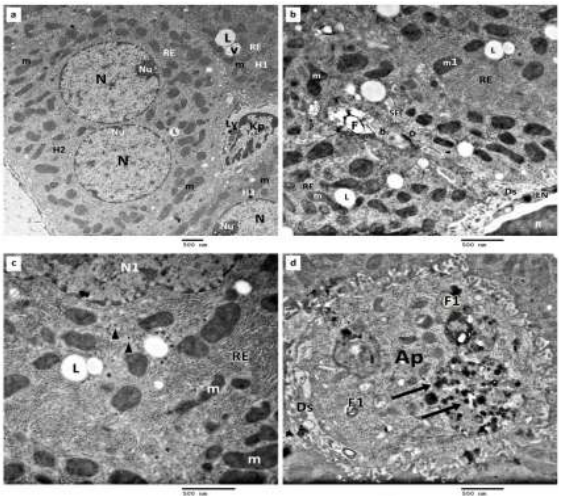

Figure 14. Electron micrographs of mouse liver of the sixth group, received repeated doses of (200 µg/kg) chitosan-capped AuNPs. **(a-c)** Cytoplasm of hepatocytes reveals proliferated endoplasmic reticulum where sER (SE) is slightly dilated. Bizarre shaped mitochondria (m) and dense mitochondria with unapparent cristae (m1) are seen. **(a)** Electron micrograph shows three adjacent hepatocytes. One hepatocyte (H1) reveals denser cytoplasm compared to the adjacent hepatocyte (H2). Notice nuclei (N) with marginated nucleoli (Nu) in hepatocytes (H2& H3). Von Kupffer cell (Kp) with lysosomes (Ly) having electron dense material is seen lining a blood sinusoid. **(b)** Electron micrograph shows dilated bile canaliculi (b) bounded by desmosomes (D) with myelin figures (F) in the lumen. **(c)** Electron micrograph of a hepatocyte with indented nucleus (N1). Notice the presence of glycogen granules (arrow head). **(d)** Electron micrograph shows apoptotic body (Ap) in a blood sinusoid containing aggregated cytoplasmic organelles, myelin figure (F1) and an electron dense material (arrow). ER; rER, L; lipid droplet, V; vacuole, Ds; space of Disse, EN; endothelial cell, R; red blood cell. (Uranyl acetate/lead citrate stain).

treated once with 2 mg/ kg AuNPs were significantly higher than those of mice treated with 200 µg/ kg every other day for 21 days (Table 2).

mRNA expression of inflammation–related genes

Injection of citrate- and chitosan-capped AuNPs at 2 mg/kg once and left for 10 days, caused statistically significant increase of IL-1, IL-6, TNF-alpha and iNOS mRNA levels (P>0.01, P>0.05) in the liver tissue, whereas the levels of COX-2 mRNA increased in mice treated with citrate-capped AuNPs but not in chitosan-capped AuNPs treated ones (Figure 15).

In case of animals injected with 200 µg/kg of either citrate- or chitosan-capped AuNPs every other day for 21 days, the induction of mRNA expression of inflammation-related genes IL-1 and TNF-alpha was similar to controls. On the other hand, IL-6 and iNOS mRNA levels were significantly elevated after both citrate- and chitosan-capped AuNPs exposure, while the levels of COX-2 mRNA increased in mice treated with citrate-capped AuNPs only (Figure 16). The housekeeping gene, action was not changed by AuNPs treatment in all groups.

Cytogenetic studies

Chromosomal aberration assay

Chromosomal aberrations were identified in bone marrow dividing cells in all treated animals. As compared to normal metaphase plate (Figure 17a), various types of chromosomal aberrations were detected such as stickiness, end to end associations, deletions, ring chromosomes, centromeric attenuation, breaks, gaps, centromeric fusions, hypoploidy and endomitosis (Figure 17, b-f). The total number of chromosomal aberrations was counted in 1000 dividing cells per animal. The mean total chromosomal aberrations in animals treated once

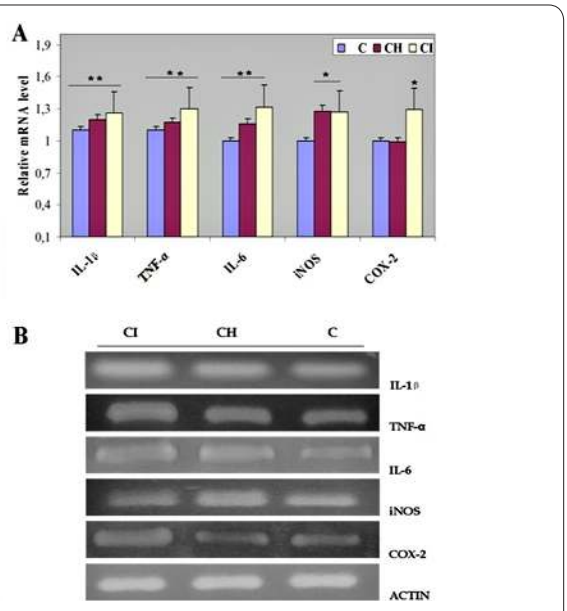

Figure 15. (A) Gene expression in groups received single dose of 2mg/kg of AuNPs by either coats, for IL1, TNF- α, IL-6, INOS, and COX- 2 mRNA in mouse liver. **(B)** mRNA transcription was detected by RT-PCR analysis using the respective primers, actin mRNA was used a housekeeping gene. CI; citrate, CH; Chitosan, C; control group (received physiological saline). Data are presented as the mean ± SD (n=3) of three independent experiments. Significant difference between groups at *p<0.05, **p<0.01.

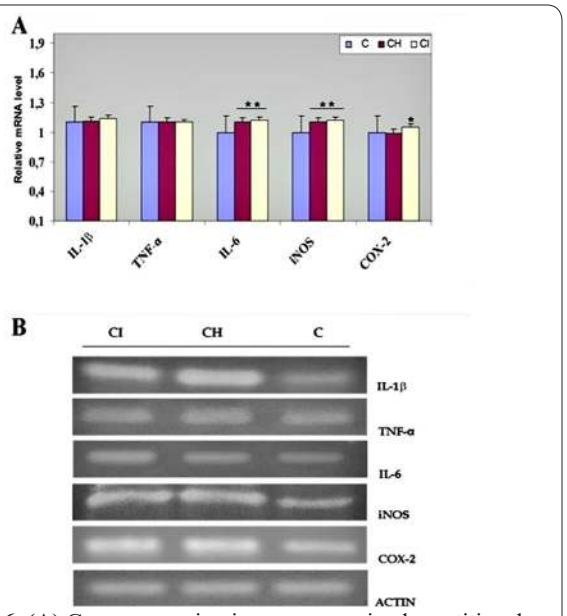

Figure 16. (A) Gene expression in groups received repetitive dose (200 µg/kg) of AuNPs by either coats, for IL1, TNF- α, IL-6, iNOS, and COX- 2 mRNA in mouse liver. **(B)** mRNA transcription was detected by RT-PCR analysis using the respective primers, actin mRNA was used a housekeeping gene. CI; citrate, CH; Chitosan, C; control (received physiological saline). Data are presented as the mean ± SD (n=3) of three independent experiments. Significant difference between groups at *p<0.05, **p<0.01.

with 2 mg/kg either citrate- or chitosan-capped AuNPs and animals treated every other day for 21 days with 200 µg/kg either citrate- or chitosan-capped AuNPs, showed significant rise when compared to negative control group but not significantly higher than positive control results (Table 3).

Non-significant increase in the frequency of abnormalities was noticed in mice treated every other day for 21 days with 200 µg/kg citrate-capped AuNPs when compared to that treated once with 2 mg/kg. On the other hand, the mean total chromosomal aberrations in mice treated for every other day for 21 days with 200 µg/kg chitosan-capped AuNPs was significantly higher than that of the group treated with 2 mg/kg as a single dose. However, non-significant difference was found between the mean total chromosomal aberrations in animals treated with citrate-capped AuNPs when compared to those of chitosan-capped AuNPs (Data not shown).

Mitotic index

The results obtained for the mitotic index (MI) showed that, there were no significant differences in values of mitotic indices in mice treated with a single dose (2 mg/kg) of either citrate-capped AuNPs (6.60± 0.82)

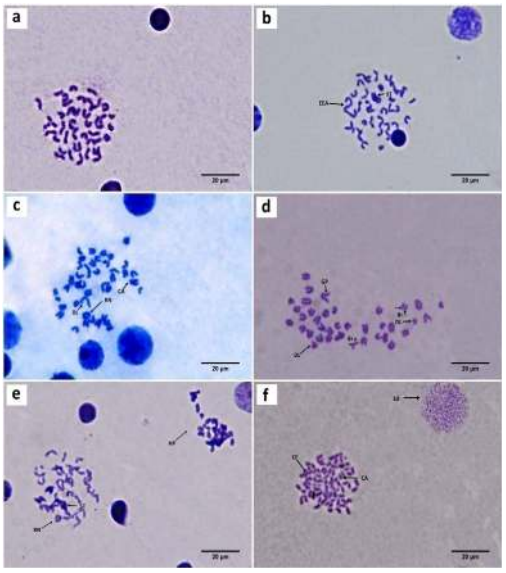

Figure 17. Photomicrograph of metaphase complements showing normal set of chromosomes **(a)** and chromosomal aberrations like stickiness (ST), end to end associations (EEA), deletions (DL), ring chromosomes (RN), centromeric attenuation (CA), breaks (Br), gaps (GP), centromeric fusions (CF), hypoploidy (HP) and endomitosis (Ed). (Geimsa stain) **(b-f).**

Table 3. Mitotic index and chromosomal aberration of the bone marrow cells of mice exposed to single and repeated doses of citrate- and chitosan- capped AuNPs.

Groups	Single dose		Repeated doses	
	MI	CA	MI	CA
NC	8.23 ± 2.65	14.0 ± 3.61*	8.03 ± 2.67*	13.50 ± 4.09*
Citrate-capped AuNPs	6.60 ± 0.82	77.67 ± 25.74*	10.03 ± 0.90	92.33 ± 9.45*
Chitosan-capped AuNPs	6.50 ± 0.46	74.0 ± 7.21*	13.27 ± 2.15*	99.67 ± 2.89*
PC	5.97 ± 1.51	66.33 ± 27.02	6.50 ± 1.25*	71.0 ± 26.0

MI: mitotic index; CA: chromosomal aberration; NC: negative control; PC: positive control. Data was represented as mean ± SD. Significance of difference where all treated groups were compared with control group (received physiological saline) at P<0.05*.

or chitosan-capped AuNPs (6.50± 0.46) compared to the positive and negative control groups (5.97± 1.51; 8.23± 2.65), respectively. Similarly, there were no significant differences in values of MI in mice treated every other day for 21 days with 200 µg/kg of citrate-capped AuNPs (10.03 ± 0.90) compared to positive and negative control groups (6.50 ± 1.25 and 8.03 ± 2.67), respectively. While mice treated every other day for 21 days with 200 µg/kg chitosan-capped AuNPs, a significant increase in MI (13.27 ± 2.15) was recorded (Table 3). In addition, non significant differences were found between the mean MI in mice treated with citrate-capped AuNPs when compared to that of chitosan-capped AuNPs by either doses. Highly significant values of MI were recorded in mice treated with 200 µg/kg every other day for 21 days when compared with that treated once with 2 mg/kg for either coats (Data not shown).

Discussion

AuNPs have broad biomedical applications in drug delivery, gene therapy, photothermal and radio-therapy (37). Despite their huge potential benefits, insufficient information is known about their health effects. Reports have shown that synthesized NPs can circulate in the body for extended periods of time without being rejected by the body's immune system. The size, shape and surface charges of NPs are responsible for their behaviors inside the body and should be considered during synthesis and applications of AuNPs, as they may be of health risk (38).

The present framework aimed to evaluate the cyto-genotoxicity induced by AuNPs and the potential histological changes in adult Swiss albino mice, as a mammalian model. The liver was selected to evaluate the cytotoxic effect because of its major role in metabolism of foreign substances (39) as well as a significant percentage of systemically administered AuNPs are trapped predominantly in the liver and spleen (40, 41). Moreover, the primary site of AuNPs accumulation in human is the liver (42). Unfortunately, little is known about the biodistribution, accumulation and toxicity of AuNPs after repeated administration (43, 44). The biodistribution and biological processes after exposures depend on a great extent to the surface physiochemical properties (45). Therefore, the attributes of AuNPs and its coated surface charges must be examined with care to ascertain toxicities (46).

During the path of metal nanoparticle preparation, it is important to use protective agents to stabilize nanoparticles. The most common strategy is to protect the nanoparticles with protective agents that can be absorbed on or bind onto the nanoparticle surface making a coat to the nanoparticle, avoiding their agglomeration (47, 48). Metal nanoparticles can be prepared by chemical approach using reducing agents to form small metal aggregates (47). With respect to the nature of reducing agent, chemical methods may be subdivided into classical chemical, using the well-known chemical reducing substances (citrate, sodium borohydride, hydrogen, etc.) and those using non deleterious solvent and naturally occurring reducing agent such as polysaccharides or plants extracts (48). Thus, this study aimed to evaluate the toxic effect of AuNPs prepared by two different reducing agents, giving the AuNPs two coats of two different natures. Citrate; a chemical anionic coat (41) and chitosan; a natural polysaccharide cationic coat (49). In addition, this study was targeted to test pro- inflammatory genes expression in the liver. Expression of pro-inflammatory genes might indicate ROS (reactive oxygen species) release. ROS stimulate the transcription of pro-inflammatory genes to produce cytokines (50&51).

The genotoxic effect of AuNPs on bone marrow cells, as it did not take much concern in research work. One of the ways to test the genotoxicity of a pharmaceutical is by testing its clastogenecity. This refers to the formation of breaks in chromosomes, which results in sections of a chromosome being deleted or rearranged giving rise to chromosomal abnormalities. These abnormalities contribute significantly to genetic diseases, congenital anomalies and malignancies. Thus, the term clastogen is used for agents giving rise to structural chromosomal aberrations (52). The reason for choosing mice in the present work, and not rats, is that mice are generally more sensitive than rats in performing genotoxic tests (35, 53).

In this study, citrate-capped AuNPs were synthesized with sizes ranging from 80-100 nm using conventional techniques for aqueous synthesis of AuNPs involving Turkevitch process of reduction of Au(III) with trisodium citrate (54). This process gives uniform and fairly spherical particles (24, 55). Citrate caps the AuNPs through the negatively charged carboxylate groups in a way to counter balance the attraction forces between colloidal particles in liquids providing the particles with Coulombic repulsion. Thus, citrate forms a negatively charged layer around the colloidal particles (56). Chitosan-coated AuNPs were prepared by reducing $HAuCl_4$ solution in the presence of chitosan. The ability of chitosan to complexate with gold originates from NH_2-groups present in the β-(1-4)-glucosamine units of the polymer. Its hydroxyl groups also interact with metal, but to lesser extent (57, 58).

The color change of the gold solution during preparation was from pale yellow to red or purple due to the Surface Plasmon Resonance (SPR). The plasmon absorption spectra of prepared AuNPs were measured by UV-visible spectrophotometer and the results obtained revealed that, the plasmon absorption of prepared AuNPs was clearly visible and their maximum absorption peaks were at 550 nm and 548 nm for citrate and chitosan- capped AuNPs respectively. These results were in accordance with a previous study carried out by Link and El-Sayed (59). They revealed that the plasmon absorption studied for 9, 15, 22, 48, and 99 nm AuNPs in aqueous solution was 517, 521, 533, and 575 nm respectively. In addition, Pedersen and Duncan (60), also found that the plasmon absorption for a "cherry red" gold nanoparticle solution was between 510 - 575 nm with a peak equal to 517.87 nm. Zeta potential of AuNPs was determined using nano zeta sizer particle analyzer, to estimate the surface charge of nanoparticles in solution (+ 30.9 mV ± 4.8). The zeta potential of citrate-capped AuNPs was (-16.7 mV) and of chitosan-capped AuNPs was (23.9 mV), indicating their negative and positive charge respectively.

The particle size distribution of AuNPs in solution was determined using particle size analyzer. Results

showed that the mean particle sizes were of 93.18 nm and 97.14 nm for citrate-capped AuNPs and chitosan-capped AuNPs respectively, with polydispersity index of 0.504 and 0.534 respectively. Polydispersity index less than 1 indicates the homogeneous nature of the formulation (61). The TEM of the prepared citrate-capped AuNPs showed that the particles were completely spherical in shape with smooth surface within the size range of (70.6-90.8 nm) and the prepared chitosan-capped AuNPs were also spherical in shape with smooth surface within the size range of (76.6-97.6 nm).

The light microscopic examination of liver tissues of the animals treated with single dose of citrate-capped AuNPs revealed vacuolation of the hepatocytes' cytoplasm and cellular swelling. This pattern of hydrobic changes occurs in vacuolar degeneration as a result of exposure to injurious substances (62). Nanoparticles are able to enter cells and interact with subcellular structures. Oxidative stress is usually a response to cell injury (50, 63). Many *in vivo* and *in vitro* studies suggested that nanoparticles of various compositions (fullerenes, carbon nanotubes and quantum dots) create ROS (64). Similarly, it was reported that AuNPs increase ROS and deplete antioxidant enzyme suggesting that oxidative stress is the major mechanism responsible for the toxic manifestations of AuNPs (65, 66). Thus, the swelling of liver cells could be attributed to the presence of ROS which damage the energy-dependent ion pumps in the plasma membrane leading to intracellular accumulation of sodium with consequent entry of water into the cells (62).

In addition, the light microscopic examination of mice treated with single dose of citrate-capped AuNPs, showed hypereosinophilic and dark homogenous cytoplasm together with margination of chromatin, karyolytic and pyknotic nuclei indicating that the cells were undergoing degeneration and apoptosis (62). NPs create ROS that modulate intracellular calcium concentrations through activation of macrophages. ROS and calcium depletion stimulate the transcription of pro-inflammatory genes to produce cytokines producing inflammation and tissue damage (67). Tissue damage will induce more cytokine production which will lead to more inflammation (68). Thus, inflammation is controlled by a complex series of intracellular and extracellular events. These hydrobic and nuclear changes in hepatocytes were also reported by Abdelhalim and Jarrar (69) who exposed rats to AuNPs with different sizes (10, 20 and 50 nm) for 3 or 7 days.

It was also observed, that in many areas narrow blood sinusoids were noticed and in other areas wide ones were seen. This could be due to the quickly removing of dead degenerated cells by phagocytic system, disappearance of these cells makes bridging, so portal tracts and central veins come nearer to each other and blood sinusoids become narrower or even obliterated in these areas. On the other hand, far blood sinusoids become dilated to overcome this faced obstruction. All these lead to distortion of liver architecture; so called lobular disarray. Increased binucleated cells were noticed, which is a sign of regeneration, in a trial to compensate for the cell loss (62, 70). Moreover, Von Kupffer cell hyperplasia and infiltration of the portal tracts with inflammatory cells, together with congestion and dilatation of the branches of the portal vein were noticed. These all are signs of inflammation in liver tissue (62). These inflammatory changes were also found by other researchers when different sizes of AuNPs on liver tissue were studied. Inflammation might be attributed to ROS induced by AuNPs (69). Besides, bile duct dilatation and proliferation were prominent microscopic findings. Such findings are present in extrahepatic biliary obstruction, but also observed in some liver diseases caused by infectious or toxic agents (71). It might be due to an increase in the mitotic activity of bile ducts with a corresponding increase of their number (72). In mice treated with a single dose of chitosan-capped AuNPs, similar findings were revealed to those treated with citrate-capped AuNPs, but only in the form of isolated affection dispersed all over the liver tissue with preserved liver architecture in most areas.

Electron microscopic examination of the liver tissue of groups received single dose of AuNPs, goes hand in hand with the findings revealed by the light microscope. It revealed changes involving both cytoplasm and nuclei. In animals treated with a single dose of citrate-capped AuNPs, rarefaction of the cytoplasm of many hepatocytes was noticed. This could be a result of the cellular swelling (vacuolar degeneration). On the other hand, in chitosan-capped AuNPs single dose-treated mice the cytoplasm appeared denser in some hepatocytes and lighter in others revealing the dark-light cell phenomena. This phenomenon was demonstrated in experimentally damaged livers and has been interpreted as a pathological change by hepatotoxic agents (73, 74).

The mitochondria in mice treated once with AuNPs were bizarre in shape; some were swollen while others were dense with unapparent cristae. These findings were in accordance with Pan et al., (75) who considered the mitochondria to be the major cell organelle that can be deleteriously affected by NPs' toxicity. This might also be due to oxidative stress produced by NPs, where excessive oxidative stress may induce an excessive or prolonged increase in mitochondrial permeability (76, 77). The stress response was the predominant factor in mitochondrial changes leading to increased ROS, mitochondrial cytochrome-c release and mitochondrial damage. Moreover, Ghadially, (74) stated that the entry of water or solutes into the mitochondria causes its enlargement and swelling. Numerous toxic agents can lead to cell damage and death by this mechanism.

Endoplasmic reticulum showed proliferation with dilatation of sER and partial degranulation of rER. Degranulation of the rER was also noticed by other researchers in hepatocytes exposed to hepatonoxious drugs (74, 78). The noticed proliferation of sER might be due to degranulation of rER. In addition, proliferation and dilatation of sER occur in a trial to metabolize and detoxify drugs and carcinogens (79). Ghadially, (74) stated that similar pictures appear in the liver on administration of hepatocarcinogens like aflatoxins and carbon tetrachloride. Furthermore, it was stated that the endoplasmic reticulum responds very early when the cell is injured; it swells due to an intake of water (74). Mitochondrial swelling together with endoplasmic reticulum swelling, constitute the major changes in cloudy swelling (74). ROS and NPs themselves expose the cell to a stressful situation. This leads to what is cal-

led endoplasmic reticulum stress; where impairment in rER function occurs, resulting in the accumulation of unfolded or misfolded proteins. To overcome this, the cell expands their ER volume. Severe or long-lasting stress favors activation of a proapoptotic module that leads to cell death (80).

The present work also revealed electron dense material most probably AuNPs in lysosomes of hepatocytes and Von Kupffer cells in mice treated once with AuNPs. AuNPs reveal high electron density and are highly homogenous in shape. This helped their ease identification among other cellular components on using TEM (81). Such finding came in agreement with other studies, which found AuNPs in endosomes and lysosomes of hepatocytes and Von Kupffer cells (82). Dilated bile canaliculi with few microvilli protruding into their lumen were seen in the present study. This might be due to stasis. In addition, white blood cells were seen in blood sinusoids and in between hepatocytes. This might indicate the occurrence of inflammation to the liver tissue (83).

Some of the hepatocytes' nuclei, in mice treated once by AuNPs with either coats, were shrunken with irregular outline and dense chromatin. These changes occur when the cell is undergoing pyknosis. In animals treated with a single dose of chitosan-capped AuNPs, some hepatocytes' nuclei showed margination of heterochromatin. This appears to be an early change that occurs in the nucleus after irreversible injury leading to cell death. In addition, margination of nucleoli was also noticed in this group. Nucleolar margination is a sign of increased protein synthesis and is frequently seen in variety of cancer cells (78, 84). The histological picture of animals treated once with AuNPs, suggests that both citrate- and chitosan-capped AuNPs produce noxious effects to the liver. This might be because AuNPs interact with proteins and enzymes of the hepatic tissue interfering with the antioxidant defense mechanism and leading to ROS generation which in turn may induce stress in the hepatocytes to undergo atrophy and death (6). The appearance of apoptotic bodies containing aggregated cytoplasmic organelles inside blood sinusoids, in these groups, denotes the fact that hepatocytes were subjected to cell death by apoptosis (78).

The histological alterations in the liver structure of the animals treated with a single dose of AuNPs in the present study were confirmed by the biochemical results. Serum liver enzyme levels (AST, ALT) showed a significant rise in animals treated by either coats of AuNPs when compared to the control one. It is known that in some diseases such as hepatitis the serum liver enzyme levels (AST, ALT) increase (85). Similarly, Zahng et al. (86) documented a significant increase in AST and ALT levels in mice injected i.p by PEG-coated AuNPs. They stated that the increase in ALT indicates damage to liver cells. As ALT and AST are mainly distributed in liver cells, and their serum levels rise with death of liver cells, thus the serum levels of these enzymes correspond well with the extent of liver cell damage, and are commonly used as indicators of liver function (86).

Regarding, the light microscopic results of animals treated with repeated doses of AuNPs with either caps, they were nearly similar, presenting, almost preserved liver architecture. Few focal areas showed findings similar to those of the animals treated with a single dose but to a lesser extent. This goes in parallel with the biochemical results. This is in accordance with the work of Lasagna-Reeves et al. (27) who, stated that no evidence of liver toxicity was observed when different doses of AuNPs (40, 200, and 400 μg/kg/day) were administrated intraperitonealy in mice every day for 8 days. Similarly, when male Sprague Dawley rats were repeatedly intravenously treated with colloidal suspensions of 14 nm AuNPs weekly for 7 weeks, followed by a 14-day washout period, histopathological examination showed no hepatotoxicity (87).

For the electron microscopic findings of the animals treated every other day for 21 days, changes in the ultrastructure of the liver tissue were similar to those treated with a single dose but to a lesser extent. This might be an indication that AuNPs when given in smaller doses on a longer duration produce less affection to liver tissue compared to its toxic effect when given in a large single dose. While liver tissues in mice treated with a single dose of citrate-capped AuNPs are more affected than those in chitosan-capped AuNPs. This emphasizes the idea that the citrate; the chemical anionic coat might be more toxic to liver tissue than the chitosan; the natural polymer cationic coat. On the other hand, in animals treated with repetitive doses, no great differences were noticed between the toxicity produced in anionic charged citrate-capped AuNPs group and those in cationic charged chitosan-capped AuNPs group. These results were in agreement with the results of Yang et al., (12) and Masotti et al., (88). A study by Goodman et al. (89) investigated the hazardous effect of AuNPs modified with an amine and carboxyl groups on several cell lines. Their results showed that anionic AuNPs species were non-toxic to cells, whereas cationic species can cause moderate toxicity in all cells lines. Another report carried out by Schaeublin et al. (90) has shown that both cationic and anionic AuNPs were toxic to cells. They revealed that both positively and negatively charged AuNPs can alter the mitochondrial membrane potential resulting into oxidative stress. The oxidative stress according to Oikawa et al. (91) enhances the production of reactive oxygen species, various immunologic stimuli and inflammation. Apart from these, the anionic and cationic surface charges of AuNPs can stimulate lymphoid cell phagocytosis to an extent greater than neutral AuNPs (92).

RT-PCR analysis of inflammation-related genes showed that results of both groups treated with a single dose of AuNPs revealed a significant rise in relative mRNA levels when compared to the control. Where, relative levels of IL-1ß, TNF-α, IL-6, iNOS and COX-2 mRNA in citrate-capped treated animals were significantly higher than the control. On the other hand, in animals treated with a single dose of chitosan-capped AuNPs, only levels of IL-1ß, TNF-α, IL-6 and iNOS were significantly higher than the control group. Also, significant rise in levels of mRNA of IL-1ß, TNF-α, IL-6 and COX-2 in animals treated with a single dose of citrate-capped AuNPs when compared to animals treated with a single dose of chitosan-capped AuNPs was recorded. This expression of mRNA of different inflammatory cytokine genes might be due to their exposure to AuNPs, which lead to transcription of pro-inflammatory

genes as a result of ROS production (6). The expressed pro-inflammatory genes' mRNA will be translated to inflammatory cytokines leading to more inflammation of the liver. Thus, AuNPs in groups treated with a single dose, induce inflammation to liver cells which is more prominent in citrate-capped AuNPs groups. These results are concomitant with the biochemical and histological findings of this work. These results are similar to what Khan et al. (8) proved, as they studied the effects of AuNPs on expression of IL-1ß, IL-6 and TNF-α in rat liver. Real-time PCR analysis showed that AuNPs significantly increased cytokine gene expression on day 1 and this had subsided by day 5. Whereas the animals treated with repeated doses revealed that, relative mRNA levels of IL-6, iNOS, and COX-2 in animals exposed to citrate-capped AuNPs were significantly higher than the control. While in animals exposed to chitosan-capped AuNPs, levels of IL-6 and iNOS only were significantly higher than the control. Comparing animals treated with citrate-capped AuNPS to those of chitosan, a significant rise in relative levels of mRNA of COX-2 was noticed. Thus, repetitive doses of AuNPs induced inflammation to liver cells which was slightly more prominent in animals exposed to citrate-capped AuNPs, as more inflammatory genes were expressed. When comparing this with the biochemical results, it was found that the animals treated with repetitive doses showed no significant rise in liver enzymes. This findings assumes that detecting pro-inflammatory genes is a more accurate method for assessing the inflammatory impact of NPs and drugs generally on different tissues than detecting serum biochemical markers.

The mitotic index revealed that single dose of AuNPs didn't significantly increase the rate of division compared to the control group, while the repetitive doses showed an increase in the mitotic index. This rise was only significant in chitosan-capped treated animals when compared to control group. This rise in mitotic index in animals treated by repeated doses is significantly higher than those treated by a single dose. This might be due to the prolonged exposure that leads to more cell damage and thus increases the cell division as a normal compensatory mechanism (93). It was also reported that, mitotic index increases in cancer cells, giving an indication that using AuNPs for prolonged durations might be carcinogenic (94, 95). However, the present work revealed that, there was no significant difference between mitotic index of citrate-capped AuNPs groups when compared to chitosan-capped AuNPs ones.

The chromosomal aberration test was used to detect genotoxicity of the examined materials, as it proved to be a sensitive indicator for monitoring the genotoxicity of environmental chemicals (52). All groups were compared to a negative control group and a positive control one. The positive control group received cyclophosphamide. Cyclophosphamide is a widely used antineoplastic agent, used in the treatment of various leukemias and different types of solid tumors as; breast cancer and lung cancer. It is used as a positive control due to its known clastogenic action (96, 97). *In vitro* and *in vivo* studies showed that NPs of various materials (diesel, carbon black, welding fumes, transition metals) are genotoxic in humans or rats (98). Due to the different properties of NPs, they may have unpredictable genotoxic properties. They may cause DNA damage indirectly, by promoting oxidative stress and inflammatory responses (99). Alternatively, if small enough, they may pass through cellular membranes and gain access to the nucleus where they may interact directly with DNA, causing damage (100, 101). Additionally, if nanomaterials are able to accumulate within a cell but not necessarily gain access to the nucleus, they may still come into direct contact with DNA during mitosis when the nuclear membrane breaks down, providing ample opportunity for DNA aberrations to arise (102).

The mean total chromosomal aberrations found in mice bone marrow cells of the two groups treated with a single dose of AuNPs, showed significant rise when compared to the negative control groups but when compared to the positive control group; that was treated with cyclophosphamide, the rise was not significant. This indicates that although AuNPs with both coats increased the mean total chromosomal aberrations but they are not genotoxic. Results should be significantly higher than that of positive control group to proof genotoxicity of these nanoparticles (103). This was also clear in the results of the groups treated with repetitive doses of AuNPs, as the mean total chromosomal aberrations found in mice bone marrow cells of animals treated with either citrate- or chitosan-capped AuNPs, showed significant rise when compared to negative control group but not when compared to positive control group. This rise in mean total chromosomal aberrations may be due to many factors rather than genotoxicity. It might be due to environmental conditions, mode of administration or different charges on NPs either positive or negative charges (104). In addition, the genotoxicity analysis revealed no significant difference between citrate-capped AuNPs groups when compared to chitosan-capped AuNPs groups, neither when treated with single nor repeated doses. This means that they have more or less similar impact on the genetic element. When comparing results in animals received single dose of AuNPs to those treated with repetitive doses, it was found that, repetitive doses revealed a rise in total number of chromosomal aberrations. This rise was significant only in chitosan-capped AuNPs groups. This might be contributed to the duration of administration, assuming that the longer is the duration of treatment with AuNPs the more chromosomal damage will occur rather than being dose related. However, further studies are needed to elucidate the real mechanism(s) that underline this effect. Similarly, *in vivo* genotoxicity of AuNPs has been investigated by Schulz et al. (105) by introducing single intratracheal instillation of AuNPs with different sizes in rats. Their study proved that AuNPs are not genotoxic. On the other hand, AuNPs seem to be genotoxic under *in vitro* conditions (106). Hong et al. (107) tried to study the effect of different coats of NPs on DNA and revealed that positively charged coats of iron oxide NPs resulted in increased DNA strand breaks of fibroblasts, while negatively charged coats did not show any significant genotoxicity. As an explanation for this behavior, the authors assumed that only positively charged particles penetrated the nucleus and interacted with the DNA (107).

Concerning chitosan-capped AuNPs groups, the results of the present work, revealed dilatation and hyper-

trophy of sER. This picture appears also in the liver on administration of hepatocarcinogens (74). Margination of the nucleolus which was also noticed in these groups, is a feature of malignant cells (74). These together with the increased mitotic index significantly when compare to control groups may give an indication that chitosan might be a carcinogenic substance and it must be subjected to more investigations either to proof or to rule out this issue (94, 95).

AuNPs provoked biochemical alteration and histological changes in the mice hepatocytes particularly with a single large dose. Chitosan as a natural cationic coat showed to be moderately less cytotoxic than citrate coat. AuNPs did not proof to be genotoxic by either coats with different durations of administration. However, the mean number of chromosomal aberrations was higher in the repeated doses, assuming that the longer is the duration of treatment with AuNPs the more chromosomal damage will occur rather than being dose related.

References

1. Pal SL, Jana U, Manna PK, Mohanta GP, Manavalan R. Nanoparticle: An overview of preparation and characterization. J Applied Pharm Sci 2011; 1: 228-234.
2. Mody VV, Siwale R, Singh A, Mody HR. Introduction to metallic nanoparticles. J Pharm Bioallied Sci 2010; 2: 282-289.
3. Laurent S, Forge D, Port M, Roch A, Robic C, Vander L, Muller RN. Magnetic iron oxide nanoparticles: synthesis, stabilization, vectorization, physicochemical characterizations, and biological applications. Chem Rev 2010; 110: 2574–2574.
4. Abhilash M. Potential applications of Nanoparticles. Int J Pharma Bio Sci 2010; 1:1-12.
5. Jamal SA. Application of Nanoparticles of Ceramics, Peptides, Silicon, Carbon, and Diamonds in Tissue Engineering. Chem Sci J 2013; CSJ -91.
6. Buzea C, Pacheco II, Robbie K. Nanomaterials and nanoparticles: Sources and toxicity. Biointerphases 2007; 2:17-172.
7. Xia Q, Li H, Liu Y, Zhang S, Feng Q, Xiao K. The effect of particle size on the genotoxicity of gold nanoparticles. J Biomed Mater Res A 2017; 105:710-719.
8. Khan JA, Pillai B, Das TK, Singh Y, Maiti S. Molecular effects of uptake of gold nanoparticles in hela cells. Chembiochem 2007; 8:1237-1240.
9. Wang SH, Lee CW, Chiou A, Wei PK. Size-dependent endocytosis of gold nanoparticles studied by three-dimensional mapping of plasmonic scattering images. J Nanobiotechnol 2010; 8:33.
10. Malathi S, Balakumaran MD, Kalaichelvan PT, Balasubramanian S. Green synthesis of gold nanoparticles for controlled delivery. Adv Mater Lett 2013; 4:933–940.
11. Boyles M, Krist T, Andosch A, Zimmermann M, Tran N, Casals E, Himly M, Puntes V, Huber C, Lütz-Meind U, Duschl A. Chitosan functionalisation of gold nanoparticles encourages particle uptake and induces cytotoxicity and pro-inflammatory conditions in phagocytic cells, as well as enhancing particle interactions with serum components. J Nanobiotechnol 2015; 13:84.
12. Yang PH, Sun XS, Chiu JF, Sun HZ, He QY. Transferrin-mediated gold nanoparticle cellular uptake. Bioconjugate Chem 2005; 16:494-496.
13. Amidi M, Hennink WE. Chitosan-based formulations of drugs, imaging agents and biotherapeutics. Adv Drug Deliv Rev 2010; 62:1–118.
14. Chen Z, Wang Z, Chen X, Xu H, Liu J. Chitosan-capped gold nanoparticles for selective and colorimetric sensing of heparin. J Nanopart Res 2013; 15:1–9.
15. Regiel-Futyra A, Kus-Liśkiewicz M, Sebastian V, Irusta S, Arruebo M, Stochel G, Kyzioł A. Development of noncytotoxic chitosan-gold nanocomposites as efficient antibacterial materials. ACS Appl Mater Interfaces 2015; 7:1087–1099.
16. Ing LY, Zin NM, Sarwar A, Katas H. Antifungal activity of chitosan nanoparticles and correlation with their physical properties. Int J Biomater 2012; 12:632- 698.
17. Iyer AK, Khaled G, Fang J, Maeda H. Exploiting the enhanced permeability and retention effect for tumor targeting. Drug Discov Today 2006; 11:1812–1818
18. Balasubramanian SK, Jittiwat J, Manikandan J, Ong CN, Yu LE, Ong WY. Biodistribution of gold nanoparticles and gene expression changes in the liver and spleen after intravenous administration in rats. Biomaterials 2010; 31:2034.
19. Guglielmo CD, Lapuente JD, Porredon C, Ramos-Lopez D, Sendra J, Borr M. *In vitro* safety toxicology data for evaluation of gold nanoparticles-chronic cytotoxicity, genotoxicity and uptake. J Nanosci Nanotechnol 2012; 12:685.
20. Cardoso E, Rezin GT, Zanoni ET, de Souza Notoya F, Leffa DD, Damiani AP, Daumann F, Rodriguez JC, Benavides R, da Silva L, Andrade VM, da Silva Paula MM. Acute and chronic administration of gold nanoparticles cause DNA damage in the cerebral cortex of adult rats. Mutat Res 2014; 766:25.
21. Schulz M, Ma-Hock L, Brill S, Strauss V, Treumann S, Groters S, et al. Investigation on the genotoxicity of different sizes of gold nanoparticles administered to the lungs of rats. Mutat Res 2011; 745:51.
22. Nelson BC, Petersen EJ, Marquis BJ, Atha DH, Elliott JT, Cleveland D, Watson SS, Tseng H, Dillon A, Theodore M, Jackman J. NIST gold nanoparticle reference materials do not induce oxidative DNA damage. Nanotoxicology 2013; 7:21.
23. May S, Hirsch C, Ripp ., Bohmer N, Kaiser JP, Diener L, Wichser A, Bürkleb A, Wick P. Transient DNA damage following exposure to gold nanoparticles. Nanoscale 2018; 10:15723-15735.
24. Mcfarland AD, Haynes CL, Mirkin CA, Van Duyne RP, Godwin HA. Citrate synthesis of gold nanoparticles. J Chem Educ 2004; 81:544.
25. Bhumkar DR, Joshi HM, Sastry M, Pokharkar VB. Chitosan reduced gold nanoparticles as novel carriers for transmucosal delivery of insulin. Pharm Res 2007; 24:1415-1426.
26. Sengupta J, Datta P, Patra HK, Dasgupta AK, Gomes A. In vivo interaction of gold nanoparticles after acute and chronic exposures in experimental animal models. J Nanosci Nanotechnol 2013; 13:1660-1670.
27. Lasagna-Reeves C, Gonzalez-Romero D, Barria MA, Olmedo I, Clos A, Sadagopa-Ramanujam VM, et al. Bioaccumulation and toxicity of gold nanoparticles after repeated administration in mice. Bioaccumulation and toxicity of gold nanoparticles after repeated administration in mice. Biochem Biophys Res Commun 2010; 393:649-655.
28. Hosseinimehr SJ, Ahmadashrafi S, Naghshvar F, Ahmadi A, Ehasnalavi S, Tanha M. Chemoprotective effects of Zataria multiflora against genotoxicity induced by cyclophosphamide in mice bone marrow cells. Integr Cancer Ther 2010; 9:219-223.
29. Sayed HM, Fouad D, Ataya FS, Hassan NH, Fahmy MA. The modifying effect of selenium and vitamins A, C, and E on the genotoxicity induced by sunset yellow in male mice. Mutat Res 2012; 744:145-153.
30. Amelinckx S, van Dyck D, van Landuyt J, van Tendeloo G. Electron microscopy: principles and fundamentals. New Jersey: Wiley, 2008.
31. Carleton HM, Rab D, Wallington EA. Carleton's histological technique. 5thed. Oxford: Oxford University Press, 1980.

32. Bancroft JD, Gamble M. Theory and practice of histological techniques. 6thed. Philadelphia: Churchill Livingstone, Elsevier, 2008.
33. Chaisera JM, Xu X. Liver function. In: Bishop ML, Fody EP, Schoeff LE (eds). Clinical chemistry: principles, techniques, and correlations, 7thed. Philadelphia: Lippincott Williams & Wilkins 2013; 519-542.
34. Win-Shwe TT, Mitsushima M, Yamamoto S, Fukushima AT, Funabashi T, Kobayashi T, et al. Changes in neurotransmitter levels and proinflammatory cytokine mRNA expressions in the mice olfactory bulb following nanoparticle exposure. Toxicol Appl Pharmacol 2008; 226: 192-198.
35. Brusick D. Principles of genetic toxicology. New York: Plenum Press, 1980.
36. Kotz S, Balakrishnan N, Read CB, Vidakovic B. Encyclopedia of statistical sciences. 2nded. Hoboken, New Jersey: Wiley-Interscience, 2006.
37. Pissuwan D, Niidome T, Cortie MB. The forthcoming applications of gold nanoparticles in drug and gene delivery systems. J Control Release 2011; 149:65-71.
38. Yah CS. The toxicity of gold nanoparticles in relation to their physiochemical properties. Biomed Res 2013; 24:400-413.
39. Munding J, Tannapfel A. Anatomy of the liver. What does the radiologist need to know? Der Radiologe 2011; 51:655-660.
40. De Jong WH, Hagens WI, Krystek P, Burger MC, Sips AJ, Geertsma RE. Particle size-dependent organ distribution of gold nanoparticles after intravenous administration. Biomaterials 2008; 29:1912-1919.
41. Yang L, Kuang H, Zhang W, Aguilar ZP, Wei H, Xu H. Comparisons of the biodistribution and toxicological examinations after repeated intravenous administration of silver and gold nanoparticles in mice. Scientific Reports 2017; 7:3303.
42. Paino IM, Marangoni VS, de Oliveir RC, Antunes LM, Zucolotto V. Cyto and genotoxicity of gold nanoparticles in human hepatocellular carcinoma and peripheral blood mononuclear cells Toxicol Lett 2012; 215:119-125.
43. Semmler-Behnke M, Kreyling WG, Lipka J, Fertsch S, Wenk A, Takenaka S, et al. Biodistribution of 1.4- and 18-nm gold particles in rats. Small 2008; 4:2108-2111.
44. Abdelhalim MA, Mady MM. Liver uptake of gold nanoparticles after intraperitoneal administration in vivo: a fluorescence study. Lipids Health Dis 2011; 10:195.
45. Gosens I, Post JA, de la Fonteyne LJ, Jansen EM, Geus JW, Cassee FR, et al. Impact of agglomeration state of nano- and submicron sized gold particles on pulmonary inflammation. Part Fibre Toxicol 2010; 7:37.
46. Verma A, Stellacci F. Effect of surface properties on nanoparticle-cell interactions. Small 2010; 6:12-21.
47. Oliveira M, Ugarte D, Zanchet D, Zarbin A. Influence of synthetic parameters on the size, structure, and stability of dodecanethiol-stabilized silver nanoparticles. J Colloid Interface Sci 2005; 292:429-435.
48. Bai J, Li Y, Du J, Wang S, Zheng J, Yang Q, et al. One-pot synthesis of polyacrylamide-gold nanocomposite. Mater Chem Phys 2007; 106:412-415.
49. Bautista-Banosa S, Hernandez-Lauzardoa A, Velázquez-del Vallea MG, Hernandez-Lopeza M, Barkab EA, Bosquez-Molinac E, et al. Chitosan as a potential natural compound to control pre and postharvest diseases of horticultural commodities. Crop Protection 2006; 25:108-118.
50. Buzea C, Pacheco II, Robbie K. Nanomaterials and nanoparticles: Sources and toxicity. Biointerphases, Biomaterials 2008; 29:1912-1919
51. Glare EM, Divjak M, Bailey MJ, Walters EH. β-Actin and GAPDH housekeeping gene expression in asthmatic airways is variable and not suitable for normalising mRNA levels. Thorax 2002; 57:765-770.
52. Sindhu Priya ES, Pate D, Venkata-Krishna K, Nagashree KS, Shyam-Prasad K, Lingaraju HB. Anticlastogenic activity of hydroalcoholic extract of mangifera indica linn. Using mammalian chromosomal aberration test in bone marrow of mice. IAJPR 2014; 4:3143-3151.
53. Frohberg H. Critique of in vivo cytogenetic test system. Inflamm Res 1973; 3:119-123.
54. Enustun BV, Turkevich J. Coagulation of colloid gold. J Am Chem Soc 1963; 85:3317.
55. Daniel MC, Astruc D. Gold nanoparticles: assembly, supramolecular chemistry, quantum-size-related properties, and applications toward biology, catalysis, and nanotechnology. Chem Rev 2004; 104:293-346.
56. Bastús GN, Merkoçi F, Piella J, Puntes V. Synthesis of highly monodisperse citrate-stabilized metal nanoparticles: kinetic control and catalytic properties. Chem Mater 2014; 26: 2836-2846.
57. Rozenberg BA, Tenne R. Polymer-assisted fabrication of nanoparticles and nanocomposites. Progress Polymer Sci 2008; 30:40-112.
58. Medina-Ramirez I, Bashir S, Luo Z, Liu J.L. Green synthesis and characterization of polymer-stabilized metal nanoparticles. Colloids and Surfaces B-Biointerfaces 2009; 73: 185-191.
59. Link S, El-Sayed M. Size and temperature dependence of the plasmon absorption of colloidal gold nanoparticles, J Phys Chem B 1999; 103:4212-4217.
60. Pedersen DB, Duncan EJ. Surface plasmon resonance spectroscopy of gold nanoparticle-coated substrates: technical report. Canada: DRDC Suffield TR, 2005.
61. Saha P, Goyal AK, Rath G. Research article formulation and evaluation of chitosan-based ampicillin trihydrate nanoparticles. Trop J Pharm Res 2010; 9:483-488.
62. Kumar V, Cotran RS, Robbins SL. Basic pathology. 9thed. Philadelphia: WB Saunders, 2003.
63. Risom L, Moller P, Loft S. Oxidative stress-induced DNA damage by particulate air pollution. Mutat Res 2005; 592:119-137.
64. Oberdörster G, Oberdörster E, Oberdörster J. Nanotoxicology: an emerging discipline evolving from studies of ultrafine particles. Environ Health Perspect 2005; 113:823-839.
65. Shrivastava R., Kushwaha P., Bhutia YC., Flora S.J. Oxidative stress following exposure to silver and gold nanoparticles in mice. Toxicology and Industrial Health 2016; 32:1391–1404.
66. Sun H, Liu Y, Bai X, Zhou X, Zhou H, Liu S, Yan B. Induction of oxidative stress and sensitization of cancer cells to paclitaxel by gold nanoparticles with different charge densities and hydrophobicities. J Mater Chem B 2018; 6:1633.
67. Brown DM, Donaldson K, Borm PJ, Schins RP, Dehnhardt M, Gilmour P, et al. Calcium and ROS-mediated activation of transcription factors and TNF-α cytokine gene expression in macrophages exposed to ultrafine particles. Am J Physiol Lung Cell Mol Physiol 2004; 286:344-353.
68. Borthwick LA, Wynn TA, Fisher AJ. Cytokine mediated tissue fibrosis. Biochimica et Biophysica Acta (BBA)-Mol Basis Dis 2013; 1832:1049-1060.
69. Abdelhalim M, Jarrar BM. Gold nanoparticles induced cloudy swelling to hydropic degeneration, cytoplasmic hyaline vacuolation, polymorphism, binucleation, karyopyknosis, karyolysis, karyorrhexis and necrosis in the liver. Lipids in Health and Disease 2011; 10:166.
70. Gerlyng P, Åbyholm A, Grotmo T, Erikstein B, Huitfeldt HS, Stokke T, Seglen PO Binucleation and polyploidization patterns in developmental and regenerative rat liver growth. Cell Proliferation

2008; 26:557–565.
71. Phyllis AS, Margaret H, Liu MH, Tavoloni N. Origin, pattern, and mechanism of bile duct proliferation following biliary obstruction in the rat. Gastroenterology 1990; 99: 466-77.
72. Burt AD, Sween RM. Bile duct proliferation—its true significance? Histopathology 1993; 23: 599-602.
73. Steiner J, Baglio CM. Electron microscopy of the cytoplasm of parenchymal liver cells in α- Naphthyl- isothiocyanate- induced cirrhosis. Lab Invest 1963;12:765.
74. Ghadially FN. Ultrastructural pathology of the cell and matrix. 2nded. London: Butterworth, 1982.
75. Pan Y, Leifert A, Ruau D, Neuss S, Bornemann J, Schmid G, et al. Gold nanoparticles of diameter 1.4 nm trigger necrosis by oxidative stress and mitochondrial damage. Small 2009; 5:2067-2076.
76. Cole NB, Daniels MP, Levine RL, Kim G. Oxidative stress causes reversible changes in mitochondrial permeability and structure. Exp Gerontol 2010; 45:596-602.
77. Huerta-García E, Pérez-Arizti JA, Márquez-Ramírez SG, Delgado-Buenrostro NL, Chirino YI, Iglesias GG, López-Marure R.Titanium dioxide nanoparticles induce strong oxidative stress and mitochondrial damage in glial cells. Free Radical Biology and Medicine 2014; 73:84-94.
78. Hyman J. Hepatotoxicity: the adverse effects of drugs and other chemicals on the liver. Philadelphia: Lippincott Williams & Wilkins, 1999.
79. Schönthal A.H. Endoplasmic Reticulum Stress: Its Role in Disease and Novel Prospects for Therapy. Scientifica 2012; 2012: 857516.
80. Malhotra JD, Kaufman RJ. The endoplasmic reticulum and the unfolded protein response, Semin. Cell Dev Biol 2007; 18:716-717.
81. Alkilany AM, Murphy CJ. Toxicity and cellular uptake of gold nanoparticles: what we have learned so far? J Nanopart Res 2010; 12:2313-2333.
82. Franco G, Dragoni S, Regoli M, Sgaragli G, Valoti M, Bertelli E. Gold nanoparticles uptake and cytotoxicity assessed on rat liver precision cut slices. Italian J Anatomy Embryol 2011; 116:78.
83. Rubin R, Strayer DS, Rubin E. Rubin's pathology: clinicopathologic foundations of medicine. 6thed. Philadelphia: Lippincott Williams & Wilkins, 2011.
84. Montironi R, Scarpelli M, Braccischi A, Galluzzi C, Diamanti L, Alberti R. Quantitative analysis of nucleolar margination in diagnostic cytopathology. Virchows Arch A Pathol Anat Histopathol 1991; 419:505-512.
85. Kim HJ, Lee HK, Cho JH. Factor analysis of the biochemical markers related to liver cirrhosis. Pakistan Journal of Medical Sciences 2015; 31:1043-1046.
86. Zhang XD, Wu D, Shen X, Liu PX, Yang N, Zhao B, et al. Size-dependent in vivo toxicity of PEG-coated gold nanoparticles. Int J Nanomedicine 2011; 6:2071-2081.
87. Rambanapasi JR, Zeevaart H, Buntting C, Bester D, Kotze C, Hayeshi R, Grobler A. Bioaccumulation and Subchronic Toxicity of 14 Nm Gold Nanoparticles in Rats, Molecules 2016; 21:763.
88. Da Sacco L, Masotti A. Chitin and chitosan as multipurpose natural polymers for groundwater arsenic removal and AS2O3 delivery in tumor therapy. Mar Drugs 2010; 15 :1518-1525.
89. Goodman CM, Mccusker CD, Yilmaz T, Rotello VM. Toxicity of Gold Nanoparticles Functionalized with Cationic and Anionic Side Chains. Bioconjugate Chem 2004; 15: 897-900.
90. Schaeublin NM, Braydich-Stolle LK, Schrand AM, Miller JM, Hutchison J, Schlagera JJ, Hussain SM. Surface charge of gold nanoparticles mediates mechanism of toxicity. Nanoscale 2011; 4:410-420.
91. Oikawa D, Akai R, Tokuda M, Takao I. A transgenic mouse model for monitoring oxidative stress. Scientific report 2012; 2:229.
92. Arnid-Malugina A, Ghandeharia H. Cellular uptake and toxicity of gold nanoparticles in prostate cancer cells: a comparative study of rods and spheres. J Appl Toxicol 2010; 30: 212-217.
93. Fox JG, Barthold S, Davisson M, Newcomer CE, Quimby FW, Smith A. The mouse in biomedical research, normative biology, husbandry, and models. 2nded. New York: Academic Press, 2006.
94. Lipponen P. Mitotic indexes as indicators of malignancy in human tumors. Int J Oncol. 1992; 1: 387-392.
95. Reece JB, Urry LA, Cain ML, Wasserman SA, Minorsky PV, Jackson RB, et al. Campbell biology in focus.1sted. San Francisco: Benjamin Cummings, 2014.
96. Hosseinimehr SJ, Karami M. Chemoprotective effects of captopril against cyclophosphamide-induced genotoxicity in mouse bone marrow cells. Arch. Toxicol. 2005; 79:482–486.
97. Samia AA, Mostafa MA, Heba SK, Sahar SM, Eman IZ. Study of the genotoxic effect of cyclophosphamide on albino Mice bone marrow polychromatic erythrocytes and the protective effect of captopril. Bull Alex Fac Med 2008; 44: 4-10.
98. Donaldson K, Tran L, Jimenez LA, Duffin R, Newby DE, Mills N, et al. Combustion-derived nanoparticles: a review of their toxicology following inhalation exposure part. Fibre Toxicol 2005; 2:10.
99. Gojova A, Guo B, Kota RS, Rutledge JC, Kennedy IM, Barakat AI. Induction of inflammation in vascular endothelial cells by metal oxide nanoparticles: effect of particle composition. Environ Health Perspect 2007; 115:403-409.
100. Nabiev I, Mitchel S, Davies A, Williams Y, Kelleher D, Moore R, et al. Nonfunctionalized nanocrystals can exploit a cell's active transport machinery delivering them to specific nuclear and cytoplasmic compartments. Nano Lett 2007; 7:3452-3461.
101. Singh N, Manshian B, Jenkins GJ, Griffiths SM, Williams PM, Maffeis TG, et al. NanoGenotoxicology: the DNA damaging potential of engineered nanomaterials. Biomaterials 2009; 30:3891-3914.
102. Donaldson K, Stone V. Current hypotheses on the mechanisms of toxicity of ultrafine particles. Ann Ist Super Sanita 2003; 39:405-410.
103. Luo Q, Li Y, Zhang Z. A systematic assessment of genotoxicity on pivaloylacylation-7ADCA-a wide existing antibiotic impurity. Int J Clin Exp Med 2014; 7:4260-4271.
104. Klien K, Godnić-Cvar J. Genotoxicity of metal nanoparticles: focus on in vivo studies genotoxicity of metal nanoparticles. Arh Hig Rada Toksikol 2012; 63:133-145.
105. Schulz M, Ma-Hock L, Brill S, Strauss V, Treumann S, Groters S, et al. Investigation on the genotoxicity of different sizes of gold nanoparticles administered to the lungs of rats. Mutat Res 2011; 22:745-751.
106. Johnston HJ, Hutchison G, Christensen FM, Peters S, Hankin S, Stoe V. A review of the in vivo and in vitro toxicity of silver and gold particulates: particle attributes and biological mechanisms responsible for the observed toxicity. Crit Rev Toxicol 2010; 40:328-346.
107. Hong SC, Lee JH, Lee J, Kim HY, Park JY, Cho J, et al. Subtle cytotoxicity and genotoxicity differences in superparamagnetic iron oxide nanoparticles coated with various functional groups. Int J Nanomedicine 2011; 6:3219-3231.